

Mixed-State Topology in Non-Hermitian Systems

Shou-Bang Yang,¹ Pei-Rong Han,² Wen Ning,¹ Fan Wu,¹ Zhen-Biao Yang,^{1,*} and Shi-Biao Zheng¹

¹*Fujian Key Laboratory of Quantum Information and Quantum Optics,
College of Physics and Information Engineering,
Fuzhou University, Fuzhou, Fujian, 350108, China*

²*School of Physics and Mechanical and Electrical Engineering, Longyan University, Longyan, China*

Non-Hermitian (NH) systems, owing to the existence of exceptional point (or ring and surface), exhibit exotic topological features which are inaccessible in Hermitian systems. While current studies on NH topology has primarily focused on pure states at zero temperature, the topological properties of mixed states remain largely unexplored. In this work, we investigate the mixed-state topology in two-dimensional NH systems using the Uhlmann phase and the thermal Uhlmann-Chern number, both structured via the Uhlmann connection at specific temperatures, revealing distinct topological characteristics compared to those of pure states. Furthermore, we extend our analysis to mixed states in three-dimensional Abelian and four-dimensional non-Abelian NH systems, confirming the existence of the higher-order mixed-state topology. Our study establishes a conceptual and practical pathway for exploring topological phenomena in the mixed-state regime of NH physics.

I. INTRODUCTION

The discovery of topological insulators [1–12] has sparked intense interest in uncovering topological nature of quantum materials. This topology is well characterized by the Berry phase [13], acquired during cyclic adiabatic evolution of a quantum state in momentum or parameter space [14, 15], which is purely geometric in origin. The local curvature in momentum or parameter space, integrated over a closed surface, yields another quantized topological invariant, the first Chern number [14–19]. As a global topology, the Chern number characterizes a system’s topological class and gives rise to observable effects like quantized Hall conductance [5–8]. Recent years have witnessed significant theoretical and experimental progress in probing topological properties across diverse physical systems, including superconducting circuits [15, 20, 21], atomic systems [22–24], and photonic systems [25–27]. However, most of these studies isolate quantum systems from their surrounding environment to minimize decoherence effects.

Non-Hermitian (NH) systems, encompassing both unitary and dissipative (gain-and-loss) physics, exhibit distinctive features absent in Hermitian cases, including spectral transitions [28–31], symmetry [32–40], dynamical effects [41–44], entanglement transitions [45], sensitivity enhancement [46, 47] and NH topology [48–51]. The rich phenomenology of NH systems is closely tied to exceptional points (EPs), where both eigenenergies and eigenstates coalesce [50–52]. Furthermore, the discovery of the extension of EPs, such as exceptional rings (ERs) [53–61] and exceptional surfaces (ESs) [62–64]- has greatly expanded the scope of NH physics.

On the other hand, when the thermal noise effect from the environment is considered, an NH quantum system is described as a mixed state at finite temperature [65].

Recently, mixed-state physics and applications have attracted extensive interest, covering topics such as protected symmetry [66–74], quantum error correction [75–77], quantum encoding [78–80], topology [81–95] and spontaneous symmetry breaking [96–103]. The topology of mixed states can be probed via the Uhlmann connection, a geometric extension of the Berry connection to density matrices [104–106]. The Uhlmann phase, accumulated during cyclic evolution of the density matrix in a Uhlmann process, serves as a finite-temperature topological indicator [107–114]. Numerous theoretical studies on the Uhlmann phase and mixed-state topology have been proposed [115–125], and the experimental measurement of the Uhlmann phase has also been demonstrated [126]. Nevertheless, their exploration in NH systems remains largely unexplored.

We first construct a two-dimensional (2D) NH system featuring an exceptional ring (ER), arising from unitary dynamics combined with both dissipative and thermal environmental effects. The topology of the ER is characterized by the Uhlmann phase and the thermal Uhlmann-Chern number [117, 118], both of which reveal exceptional features distinct from the those in open systems with pure NH effects. We then extend our investigation of such exceptional topology to higher dimensions. In a 3D NH system [48], we introduce a thermal Dixmier-Douady (DD) invariant to characterize its finite-temperature topology. For a 4D non-Abelian NH system [49], we analyze the Uhlmann phase and the second thermal Uhlmann-Chern number, both of which demonstrate higher-order topological features at finite temperatures. Our work advances the understanding of mixed-state topology in higher-dimensional systems by unifying NH physics and quantum geometry.

* zbyang@fzu.edu.cn

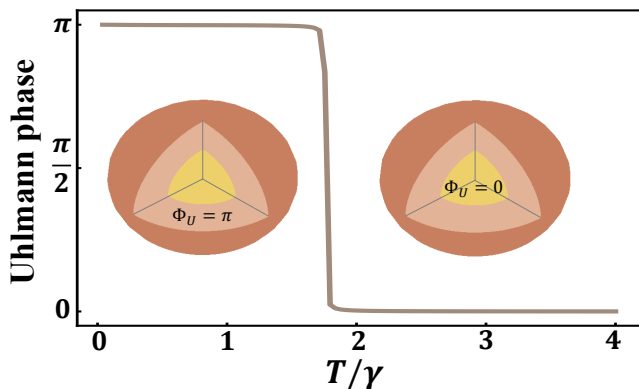


FIG. 1. The Uhlmann phase Φ_U as a function of temperature T , which scales with γ .

II. MIXED-STATE TOPOLOGY OF THE 2D NH SYSTEM

A. The Uhlmann phase

We consider a generic two-level system with particle gain and loss, the Hamiltonian is (setting $\hbar = 1$)

$$H = \sum_{\nu=x,y,z} q_\nu \sigma_\nu + i\gamma \sigma_z, \quad (1)$$

where σ_ν are Pauli matrices, q_ν the corresponding control parameters and γ the gain-loss rate. The eigenenergies of Eq. (1) are $E = \pm\sqrt{\Omega^2 - \gamma^2}$, with $\Omega = \sqrt{q_x^2 + q_y^2 + q_z^2}$.

When $\Omega = \gamma$, the two eigenenergies coalesce, and the exceptional point (EP), originally located at the center of the Bloch sphere ($\gamma = 0$), expands into an ER of radius γ in the $\{q_x, q_y\}$ plane (taking $q_z = 0$), giving rise to intriguing topological properties.

We now focus on mixed-state topology, which can be probed via the Uhlmann phase. To this end, we construct a parameter loop in the $\{q_x, q_z\}$ plane to encircle the ER. The controlled Hamiltonian in (1) is parameterized as $\{q_x, q_y, q_z\} = \{r \sin \theta + d, 0, r \cos \theta\}$, where $d = 5\gamma/2$ denotes the displacement of the loop center along the q_x direction and $r = 2\gamma$ is the loop radius. The eigenenergies and eigenstates are denoted by $E_{1,2}$ and $|u_{1,2}\rangle$, respectively. The corresponding normalized left eigenstates $\langle u_{1,2}^L|$ satisfy $\langle u_n^L|H_2 = \langle u_n^L|E_n$ and $\langle u_m^L|u_n\rangle = \delta_{mn}$. At finite temperature T , the mixed-state density matrix is expressed as

$$\rho = \sum_{n=1,2} P_n |u_n\rangle \langle u_n^L|, \quad (2)$$

with Boltzmann weights $P_n = e^{-E_n/T}/Z$ and Z the partition function. As θ evolves from 0 to 4π , the eigenenergies traverse both sides of the Möbius-like energy band, while the mixed-state trajectory encircles the ER twice in parameter space. The Uhlmann connection is given by

$$A_U^\theta = \sum_{m,n}^{1,2} \frac{|u_m(\theta)\rangle \langle u_m^L(\theta)| [\partial_\theta \sqrt{\rho_\theta}, \sqrt{\rho_\theta}] |u_n(\theta)\rangle \langle u_n^L(\theta)|}{P_m(\theta) + P_n(\theta)} d\theta. \quad (3)$$

Under the parallel transport condition and using Eq. (2), this reduces to

$$\begin{aligned} A_U^\theta &= \frac{1}{2} [f(T) - f^2(T)] (|u_1\rangle \langle u_2^L| \langle \partial_\theta u_1^L| u_2\rangle - |u_2\rangle \langle u_1^L| \langle u_2^L| \partial_\theta u_1\rangle) \\ &\quad + \frac{1}{2} [3f(T) - f^2(T)] (|u_1\rangle \langle u_2^L| \langle u_1^L| \partial_\theta u_2\rangle - |u_2\rangle \langle u_1^L| \langle \partial_\theta u_2^L| u_1\rangle) \\ &= f(T) (|u_1\rangle \langle u_2^L| \langle \partial_\theta u_1^L| u_2\rangle - |u_2\rangle \langle u_1^L| \langle u_2^L| \partial_\theta u_1\rangle), \end{aligned} \quad (4)$$

where $f(T) = \left(1 - \operatorname{sech} \frac{E_1}{T}\right)$. The Uhlmann phase, determined by the holonomy of A_U^θ , is defined via the mismatch between the initial and final points:

$$\Phi_U = \arg \operatorname{Tr}(\rho_0 e^{\int A_U^\theta d\theta}), \quad (5)$$

with ρ_0 the density matrix at $\theta = 0$. Numerical simulations of Φ_U are shown in Fig. 1. For $T/\gamma < 1.95$, the phase accumulates π after two looping cycles ($2\mathcal{L}$), around the ER. In contrast, Φ_U vanishes for $T/\gamma > 1.95$, with $T/\gamma = 1.95$ marking the critical point of a topological transition. This temperature-dependent transition, absent in pure-states NH systems, highlights the interplay between thermal fluctuations and NH topology.

To further investigate this feature, we fix $T/\gamma = 0.5$ and gradually displace the parameter loop by tuning d from 0 to 4γ , as shown in Fig. 2. For $d < \gamma$, the parameter loop lies outside the ER and encircles the two EPs on the $\{q_x, q_z\}$ plane. In this case, the Uhlmann phase Φ_U behaves similarly to that in Hermitian systems: it accumulates a 2π after the mixed state evolves through one cycle consisting of two loops ($2\mathcal{L}$). When d increases to $d = \gamma$, the parameter loop crosses the ER. At this boundary ($d = \gamma$), Φ_U undergoes a transition from 2π to π , making a first topological transition. As d increases further, the loop crosses the ER and becomes intertwined with it. When the loop encircles only one EP on the $\{q_x, q_z\}$ plane, Φ_U remains π until d increases up to 3γ .

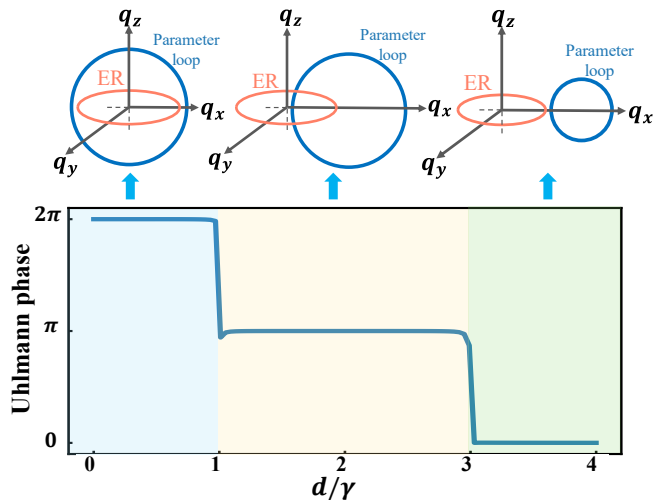


FIG. 2. The Uhlmann phase Φ_U as a function of the parameter loop displacement d , which scales with γ . Φ_U accumulates 2π , π , and 0 after one cycle with two loops of mixed-state evolution when the parameter loop encloses two EPs, encircles the ER while enclosing one EP and disengages from the ER, respectively.

At this second boundary ($d = 3\gamma$), Φ_U undergoes another topological transition, from π to 0 . For even larger d , the loop moves far away from the ER and no longer encloses it, during which Φ_U stays at zero. The twofold topological transition stands in stark contrast to the Uhlmann phase behavior observed in Hermitian systems.

B. The Thermal Uhlmann-Chern number

We now investigate the global topology characterized by the thermal Uhlmann-Chern number when the parameter space extends to a 3D sphere at finite temperatures. The Hamiltonian in Eq. (1) is parameterized by $\{q_x, q_y, q_z\} = R\{\sin\theta\cos\phi, \sin\theta\sin\phi, \cos\theta\}$, where R denotes the sphere radius. The eigenen-

ergies are $E_{1,2} = \pm\sqrt{R^2 - \gamma^2 + 2i\gamma R\cos\theta}$, and the corresponding right eigenstates are $|u_{1,2}\rangle = (R\sin\theta e^{-i\phi}, E_{1,2} - R\cos\theta - i\gamma)/N_{1,2}$, where $N_{1,2}$ is the normalization constants. The left eigenstates $\langle u_{1,2}^L|$ follow from the biorthogonal condition $\langle u_m^L|u_n\rangle = \delta_{mn}$ [45]. From Eq. (4), we obtain the Uhlmann connections A_U^θ and A_U^ϕ at temperature T . The thermal Uhlmann-Chern number is then determined by the Uhlmann curvature [117]. Importantly, unlike the Berry connection, the Uhlmann connections derived from the mixed-state density matrix are inherently matrix-valued. The Uhlmann curvature is defined as [104]

$$F_U = dA_U + A_U \wedge A_U, \quad (6)$$

and the thermal Uhlmann-Chern number is given by

$$C_U = \frac{i}{2\pi} \int \lambda(E, T) \text{Tr}(\rho F_U), 1/\lambda(E, T) = \tanh^3 \frac{E}{T}. \quad (7)$$

Substituting the Uhlmann connection from Eq. (4) into Eq. (6) and evaluating the trace with the density matrix yields

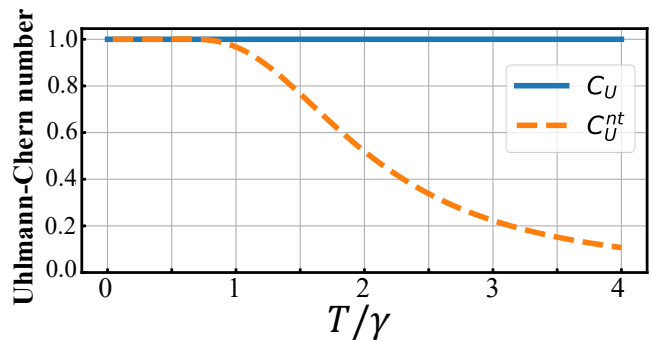


FIG. 3. The thermal Uhlmann-Chern number C_U (blue solid line) and NT thermal Uhlmann-Chern number C_U^{nt} (yellow dashed line) as functions of temperature T , which scales with γ .

$$\begin{aligned} \text{Tr}(\rho \partial_\theta A_U^\phi) &= -\text{Tr}(\rho \partial_\phi A_U^\theta) = \tanh \frac{E}{T} f(T) \frac{iR^2 \sin^2 \theta}{|N|^2} (\langle \partial_\theta u_-^L | u_+ \rangle - \langle u_+^L | \partial_\theta u_- \rangle), \\ \text{Tr}(\rho [A_U^\theta, A_U^\phi]) &= \tanh \frac{E}{T} f^2(T) \frac{iR^2 \sin^2 \theta}{|N|^2} (\langle \partial_\theta u_-^L | u_+ \rangle - \langle u_+^L | \partial_\theta u_- \rangle). \end{aligned} \quad (8)$$

Inserting the density matrix into the definition of the Chern character to construct the form

$$\text{Tr}(\rho F_U) = \tanh^3 \frac{E}{T} \frac{iR^2 \sin^2 \theta}{|N|^2} (\langle \partial_\theta u_-^L | u_+ \rangle - \langle u_+^L | \partial_\theta u_- \rangle), \quad (9)$$

and plugging this into Eq. (7), leads to $C_U = 1$. Additionally, in the presence of thermal fluctuations, a non-

topological (NT) thermal Uhlmann-Chern number can be defined, that is

$$C_U^{nt} = \frac{i}{2\pi} \int \text{Tr}(\rho F_U), \quad (10)$$

whose temperature-dependent feature is shown in Fig. 3. It clearly shows that the NT thermal Uhlmann-Chern

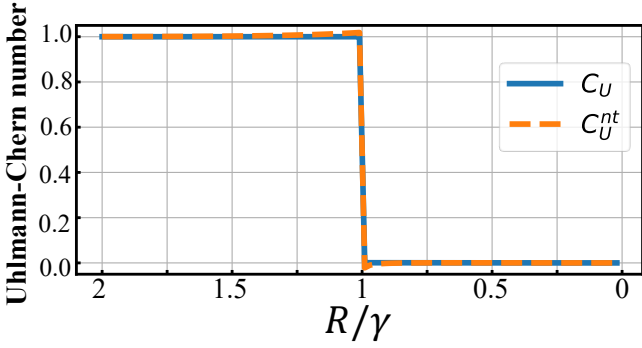


FIG. 4. The thermal Uhlmann-Chern number C_U (blue solid line) and the NT thermal Uhlmann-Chern number C_U^{nt} (yellow dashed line) as functions of the parameter sphere radius R , which scales with γ .

number C_U^{nt} drops gradually with the increase of the temperature T . This is contrast to the case of pure states in NH systems, where the Chern number remains 1.

We then show the topological transition of the thermal Uhlmann-Chern number C_U and the NT thermal Uhlmann-Chern number C_U^{nt} with respect to the radius R for the fixed temperature $T/\gamma = 0.5$. As shown in Fig. 4, both C_U and C_U^{nt} keep 1 when $R/\gamma > 1$, and abruptly vanish to 0 when crossing the critical point $R/\gamma = 1$ and finally keep 0 for $R/\gamma < 1$. Both C_U and C_U^{nt} exhibit a topological transition from the topological phase to the normal phase at the critical point $R/\gamma = 1$. The phenomenon is precluded in the Hermitian case due to the spectral properties and the orthogonality of eigenstates. The intriguing feature exhibited in variation of both C_U and C_U^{nt} versus T and R demonstrate that the topological character is jointly influenced by thermal noise and dissipation, with its effect suppressed as the system-environment coupling strengthens. The interplay of the mixed-state geometry and the NH-degeneracy advances the exotic topology inherent in such a thermal system-environment coupling mechanism.

III. MIXED-STATE TOPOLOGY OF THE 3D NH SYSTEM

For a three-level system, the NH Hamiltonian is modeled as

$$H_3 = \vec{q} \cdot \vec{\Lambda} + i\gamma\Lambda_8, \quad (11)$$

where $\vec{q} = \{\Omega_1 \cos \phi_1, \Omega_1 \sin \phi_1, \Omega_2 \cos \phi_2, \Omega_2 \sin \phi_2\}$ defines the 4D parameter space, $\vec{\Lambda} = \{\Lambda_1, \Lambda_2, \Lambda_6, \Lambda_7\}$ are the 3×3 Gell-Mann matrices [127], satisfying $[\lambda_j, \lambda_k] = if^{jkl}\lambda_l$. The term $i\gamma\Lambda_8$ introduces the non-Hermiticity. For $|\Omega_1| = \gamma/3$ and $|\Omega_2| = 2\sqrt{2}\gamma/3$, an exceptional surface (ES) composed of third-order EPs emerges in the 4D parameter space, where the eigenenergies are three-fold degenerate and the eigenstates exhibit a three-order

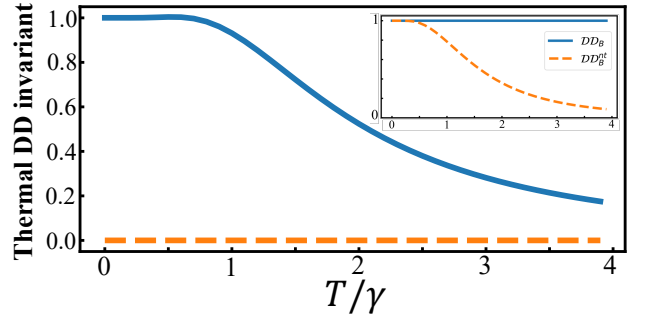


FIG. 5. The NT thermal DD invariant \mathcal{DD}_B^{nt} versus temperature T (scales with γ). The blue solid line represents the 4D parameter space enclosing the ES, while the yellow dash line corresponds to the case while the parameter space without enclosing the ES. The inset shows the Hermitian case, where the blue solid and yellow dash lines are the \mathcal{DD}_B and \mathcal{DD}_B^{nt} as functions of temperature T , respectively.

exceptional topological transition. We then construction the parameters as $\Omega_1 = R \cos \alpha$ and $\Omega_2 = R \sin \alpha$, the topological properties of the pure-state case can be characterized by the Dixmier-Douady (DD) invariant, defined as [128, 129], $\mathcal{DD} = \frac{1}{2\pi^2} \int_{S^3} \mathcal{M}_{\alpha\phi_1\phi_2} d\alpha \wedge d\phi_1 \wedge d\phi_2$, where $\mathcal{M}_{\alpha\phi_1\phi_2}$ is the three-form Berry curvature, related to the quantum metric or the two-form curvature by $\mathcal{M}_{\alpha\phi_1\phi_2} = \epsilon_{\alpha\phi_1\phi_2} \left[4\sqrt{\det(\mathcal{G}_{\alpha\phi_1\phi_2})} \right] = -\frac{1}{2} (\mathcal{F}_{\alpha\phi_1} + \mathcal{F}_{\phi_2\alpha})$. In NH systems, the quantum metric tensor and Berry curvature correspond to the real and imaginary parts of the quantum geometric tensor [48] $\chi_{\mu\nu} = \mathcal{G}_{\mu\nu} + i\mathcal{F}_{\mu\nu} = \sum_{n \neq m} \frac{\langle u_m^L | \partial_\mu H | u_n \rangle \langle u_m^L | \partial_\nu H | u_n \rangle}{(E_m^L - E_n)(E_m - E_n^L)}$, respectively, where $|u_{m,n}\rangle$ and $\langle u_{m,n}^L|$ denote the right and left eigenstates. For mixed states, we propose the thermal DD invariant, which can be obtained from the Bures metric [130]

$$\mathcal{G}_B^{\mu\nu} = \frac{1}{2} \sum_{m,n} \frac{\langle u_m | \partial_\mu \rho | u_n \rangle \langle u_n | \partial_\nu \rho | u_m \rangle}{P_m + P_n}, \quad (12)$$

where P_m and P_n are the coefficients of the system's initial state. In the Hermitian case, the mixed-state density matrix is given as

$$\rho = P_0 |u_0\rangle \langle u_0| + P_+ |u_+\rangle \langle u_+| + P_- |u_-\rangle \langle u_-|, \quad (13)$$

where $P_0 = 1/Z$ and $P_\pm = e^{\mp E_\pm/T}/Z$. The thermal three-form Berry curvature, calculated via the Bures metric, reads

$$\mathcal{M}_B = 4\sqrt{\mathcal{G}_B^{\alpha\alpha} \left(\mathcal{G}_B^{\phi_1\phi_1} \mathcal{G}_B^{\phi_2\phi_2} - |\mathcal{G}_B^{\phi_1\phi_2}|^2 \right)}, \quad (14)$$

from which we introduce the thermal DD invariant

$$\mathcal{DD}_B = \frac{1}{2\pi^2} \int_{S^3} \lambda_1(E, T) \mathcal{M}_B, \quad (15)$$

with $\lambda_1(E, T) = \frac{2\sqrt{2} \sin 2\alpha \sinh^2(E_+/2T) \sinh(E_+/T)}{\sqrt{\cosh(E_+/T)(1+2\cosh(E_+/T))^3}}$, yielding $\mathcal{DD}_B = 1$. Analogously, we introduce the NT thermal

DD invariant as

$$\mathcal{D}\mathcal{D}_B^{nt} = \frac{1}{2\pi^2} \int_{S^3} \mathcal{M}_B, \quad (16)$$

whose temperature dependence is shown in the inset of Fig. 5. The blue solid line represents $\mathcal{D}\mathcal{D}_B$, which remain unity at finite temperature, while the yellow dash line corresponds to $\mathcal{D}\mathcal{D}_B^{nt}$, which gradually decreases as the temperature rises.

In the NH case, the mixed-state density matrix at temperature T is described as $\rho = \sum_n^{1,2,3} P_n |u_n\rangle \langle u_n^L|$, where $P_n = e^{-E_n/T}/Z$, and the Bures metric is rewritten as

$$\begin{aligned} \mathcal{G}'_{B^{\mu\nu}} &= \sum_{m,n} (P_m \langle \partial_\mu u_m | u_n \rangle + P_n \langle u_m | \partial_\mu u_n \rangle) \\ &\times (P_m \langle u_n | \partial_\nu u_m \rangle + P_n \langle \partial_\nu u_n | u_m \rangle) / (P_m + P_n). \end{aligned} \quad (17)$$

As the temperature T varies, the calculated NT thermal DD invariant $\mathcal{D}\mathcal{D}_B^{nt}$ versus T is plotted against T in Fig. 5. The blue solid curve shows the result when the parameter sphere encloses the ES, in which case $\mathcal{D}\mathcal{D}_B^{nt}$ decreases from unity as T increases. The yellow dashed line shows $\mathcal{D}\mathcal{D}_B^{nt}$ versus T when the parameter sphere does not enclose the ES, where it remains zero across the entire temperature range. A topological transition, characterized by the thermal DD invariant, occurs when the parameter space crosses the ES.

IV. MIXED-STATE TOPOLOGY OF THE 4D NON-ABELIAN SYSTEM

We next investigate the mixed-state topology of the 4D non-Abelian system using the Uhlmann phase and the second Chern number [49, 131].

A. The Uhlmann phase

We consider a 4D non-Abelian system with particle gain and loss, described by the Hamiltonian

$$H_4 = \sum_{\mu=1}^5 q_\mu \Gamma_\mu + i\gamma \Gamma_4, \quad (18)$$

where Γ_μ are fourth-order Dirac matrices satisfying the Clifford algebra $\{\Gamma_m, \Gamma_n\} = 2\delta_{mn} I_0^{4*4}$ [49], and γ quantifies the strength of gain and loss. When $q_4 = 0$, the Hamiltonian (18) hosts two degenerate eigenenergies $E_\pm = \sqrt{|q|^2 - \gamma^2}$, which coalesce at $q_1^2 + q_2^2 + q_3^2 + q_5^2 = \gamma^2$, an exceptional hypersphere (EHS) on the $\{q_1, q_2, q_3, q_5\}$ subspace.

To probe the Uhlmann phase associated with such a EHS, we construct a parameterized evolution path for $\vec{q} = \{(r \sin \theta + d)/\sqrt{2}, (r \sin \theta - d)/\sqrt{2}, 0, r \cos \theta, 0\}$, with $r/\gamma = 2$ and $d/\gamma = 5/2$. This parameter

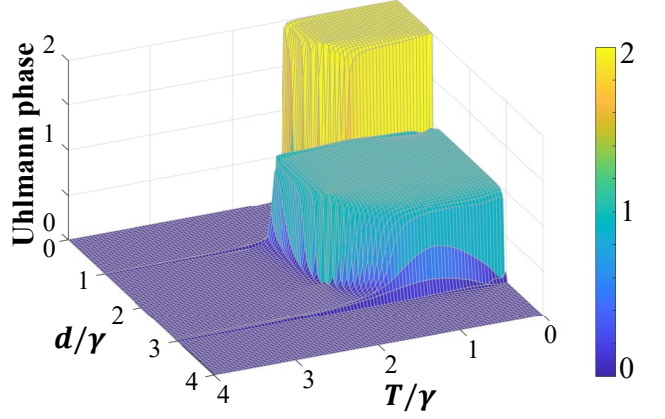


FIG. 6. The Uhlmann phase Φ_U as functions of temperature T and parameter loop displacement d , both scale with γ .

loop lies in the $\{q_1, q_3, q_5\}$ subspace and intertwines with the EHS. The eigenenergies are given by $E_{1,2} = \pm \sqrt{r^2 + d^2 - \gamma^2 + 2rd \sin \theta + 2ir\gamma \cos \theta}$, and the degenerate right eigenstates are $|u_{1,2}^\alpha\rangle = [0, r \sin \theta + d, \sqrt{2}(E_{1,2} + r \cos \theta + i\gamma), r \sin \theta + d]^T / N_{1,2}$ and $|u_{1,2}^\beta\rangle = [\sqrt{2}(E_{1,2} + r \cos \theta + i\gamma), r \sin \theta + d, 0, -(r \sin \theta + d)]^T / N_{1,2}$. The corresponding degenerate left eigenstates $\langle u_{1,2}^{L\alpha\beta}|$ are obtained by the biorthogonal condition $\langle u_{j,k}^{Lm,n} | u_{j,k}^{m,n} \rangle = \delta_{jk} \delta_{mn}$. At finite temperature T , the mixed-state density matrix is expressed as

$$\rho = \sum_{n=1,2} P_n (|u_n^\alpha\rangle \langle u_n^{L\alpha}| + |u_n^\beta\rangle \langle u_n^{L\beta}|), \quad (19)$$

where P_n represents the Boltzmann weights. The Uhlmann connection is given by

$$A_U^\theta = \sum_{m,n} \sum_{j,k}^{1,2} \frac{|u_m^j(\theta)\rangle \langle u_m^{Lj}(\theta)| [\partial_\theta \sqrt{\rho_\theta}, \sqrt{\rho_\theta}] |u_n^k(\theta)\rangle \langle u_n^{Lk}(\theta)|}{P_m(\theta) + P_n(\theta)} d\theta. \quad (20)$$

Applying the parallel transport condition to Eqs. (19) and (20) under the biorthogonal constraints yields

$$\begin{aligned} A_U^\theta &= \sum_{m \neq n} \sum_{j,k}^{1,2} \sum_{\alpha,\beta} [f(T) - f^2(T)] \langle \partial_\theta u_m^{Lj} | u_n^k \rangle |u_m^{Lj}\rangle \langle u_n^k| \\ &+ \sum_{m \neq n} \sum_{j,k}^{1,2} \sum_{\alpha,\beta} [3f(T) - f^2(T)] \langle u_m^{Lj} | \partial_\theta u_n^k \rangle |u_m^{Lj}\rangle \langle u_n^k|. \end{aligned} \quad (21)$$

Crucially, the mixed state in Eq. (19) must complete two winding loops $2\mathcal{L}$ to accumulate a well-defined Uhlmann phase

$$\Phi_U = \arg \text{Tr}(\rho_0 e^{\int A_U^\theta d\theta}) = \pi. \quad (22)$$

As shown in Fig. 6, the Uhlmann phase Φ_U drops abruptly to 0 when the temperature exceeds the critical value of $T/\gamma = 1.98$. Meanwhile, for a fixed T as d/γ

increases from 0 to 4, the Uhlmann phase exhibits twofold distinct topological transitions.

B. The second thermal Uhlmann-Chern number

To characterize the mixed-state topology via the second thermal Uhlmann-Chern number, we consider the 4D NH Hamiltonian in Eq. (18), which is associated with the five-dimensional (5D) hypersphere in the parameter space spanned by $\{\theta_1, \theta_2, \phi_1, \phi_2, R\}$, where R is the radius of the hypersphere. The generic form of \vec{q} is taken as $\vec{q} = R\{\sin \theta_1 \sin \theta_2 \cos \phi_2, \sin \theta_1 \cos \theta_2 \cos \phi_1, \sin \theta_1 \cos \theta_2 \sin \phi_1, \cos \theta_1, \sin \theta_1 \sin \theta_2 \sin \phi_2\}$ in Eq. (18). The eigenenergies and biorthogonal eigenstates are given by $E_{1,2} = \pm\sqrt{R^2 - \gamma^2 + 2i\gamma R \cos \theta_1}$, and $|u_{1,2}^\alpha\rangle = [0, R \sin \theta_1 \sin \theta_2 e^{-i(\phi_1 - \phi_2)}, (E_{1,2} + R \cos \theta + i\gamma)e^{-i\phi_1}, R \sin \theta_1 \cos \theta_2] / N_{1,2}$, $|u_{1,2}^\beta\rangle = [(E_{1,2} + R \cos \theta + i\gamma)e^{i\phi_2}, R \sin \theta_1 \cos \theta_2 e^{-i(\phi_1 - \phi_2)}, 0, -R \sin \theta_1 \sin \theta_2] / N_{1,2}$, with the corresponding degenerate left eigenstates $\langle u_{1,2}^{L\alpha\beta}|$.

At finite temperature T , the four components of Uhlmann connection derived from Eqs. (19) and (20), which extend the parallel transport condition to mixed states under non-Abelian gauge symmetry, can be expressed as

$$\begin{aligned}
A_U^{\theta_1} &= f(T) \sum_{j=\alpha,\beta} \langle u_1^j | \partial_{\theta_1} u_2^j \rangle \left(|u_1^j\rangle \langle u_2^j| - |u_2^j\rangle \langle u_1^j| \right), \\
A_U^{\theta_2} &= -f(T) \frac{R^2 \sin^2 \theta_1}{N_1 N_2} \sum_{m \neq n}^{1,2} \left(|u_m^\alpha\rangle \langle u_n^\beta| - |u_n^\beta\rangle \langle u_m^\alpha| \right), \\
A_U^{\phi_1} &= -f(T) \frac{R^2 \sin^2 \theta_1}{2N_1 N_2} \sum_{m \neq n}^{1,2} \left[\sum_{j \neq k}^{\alpha,\beta} \sin 2\theta_2 |u_m^j\rangle \langle u_n^k| \right. \\
&\quad \left. - 2 \cos^2 \theta_2 \left(|u_m^\alpha\rangle \langle u_m^\alpha| + |u_m^\beta\rangle \langle u_m^\beta| \right) \right], \\
A_U^{\phi_2} &= f(T) \frac{R^2 \sin^2 \theta_1}{2N_1 N_2} \sum_{m \neq n}^{1,2} \left[\sum_{j \neq k}^{\alpha,\beta} \sin 2\theta_2 |u_m^j\rangle \langle u_n^k| \right. \\
&\quad \left. + 2 \sin^2 \theta_2 \left(|u_m^\alpha\rangle \langle u_m^\alpha| - |u_m^\beta\rangle \langle u_m^\beta| \right) \right]. \quad (23)
\end{aligned}$$

Substituting the density matrix from Eq. (19) into the Uhlmann curvature yields

$$\text{Tr}(\rho F_U^{\theta_1 \theta_2}) = \text{Tr}(\rho F_U^{\phi_1 \phi_2}) = 0, \quad (24)$$

and calculating the first thermal Uhlmann-Chern number gives

$$C_{U1} = \frac{i}{2\pi} \int \lambda(E, T) \text{Tr}(\rho F_U) = C_{U1}^{nt} = 0, \quad (25)$$

which is consistent with results for zero-temperature non-Abelian Hermitian systems.

The second thermal Uhlmann-Chern number C_{U2} reveals a novel feature. Its general expression is

$$C_{U2} = \frac{1}{8\pi^2} \int \lambda_2(E, T) \text{Tr}(\rho F_U \wedge F_U), \quad (26)$$

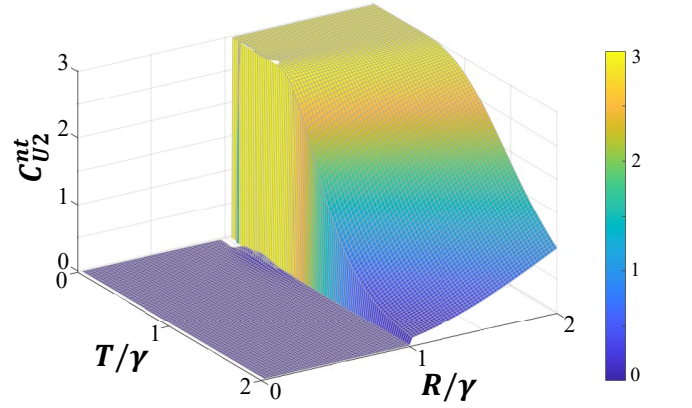


FIG. 7. The NT thermal Uhlmann-Chern number C_{U2}^{nt} versus temperature T and parameter hypersphere radius R , both scale with γ .

where F_U is the Uhlmann curvature tensor and $1/\lambda_2(E, T) = \tanh^5 \frac{E}{T}$. To compute C_{U2} , we explicitly evaluate all components of the Uhlmann curvature as follows:

$$\begin{aligned}
\text{Tr} \left[\rho \left(\partial_{\phi_1} A_U^{\phi_2} - \partial_{\phi_2} A_U^{\phi_1} \right) \left(\partial_{\theta_1} A_U^{\theta_2} - \partial_{\theta_2} A_U^{\theta_1} \right) \right] &= 4 \tanh \frac{E}{T} f^2(T) \frac{R^6 \sin^6 \theta_1 \sin 2\theta_2}{(N_1 N_2)^3} \left(\langle u_1^\alpha | \partial_{\theta_1} u_2^\alpha \rangle + \langle u_1^\beta | \partial_{\theta_1} u_2^\beta \rangle \right), \\
\text{Tr} \left[\rho \left(\partial_{\phi_1} A_U^{\phi_2} - \partial_{\phi_2} A_U^{\phi_1} \right) \left(A_U^{\theta_1} A_U^{\theta_2} - A_U^{\theta_2} A_U^{\theta_1} \right) \right] &= -2 \tanh \frac{E}{T} f^3(T) \frac{R^6 \sin^6 \theta_1 \sin 2\theta_2}{(N_1 N_2)^3} \left(\langle u_1^\alpha | \partial_{\theta_1} u_2^\alpha \rangle + \langle u_1^\beta | \partial_{\theta_1} u_2^\beta \rangle \right), \\
\text{Tr} \left[\rho \left(A_U^{\phi_1} A_U^{\phi_2} - A_U^{\phi_2} A_U^{\phi_1} \right) \left(\partial_{\theta_1} A_U^{\theta_2} - \partial_{\theta_2} A_U^{\theta_1} \right) \right] &= -2 \tanh \frac{E}{T} f^3(T) \frac{R^6 \sin^6 \theta_1 \sin 2\theta_2}{(N_1 N_2)^3} \left(\langle u_1^\alpha | \partial_{\theta_1} u_2^\alpha \rangle + \langle u_1^\beta | \partial_{\theta_1} u_2^\beta \rangle \right), \\
\text{Tr} \left[\rho \left(A_U^{\phi_1} A_U^{\phi_2} - A_U^{\phi_2} A_U^{\phi_1} \right) \left(A_U^{\theta_1} A_U^{\theta_2} - A_U^{\theta_2} A_U^{\theta_1} \right) \right] &= \tanh \frac{E}{T} f^4(T) \frac{R^6 \sin^6 \theta_1 \sin 2\theta_2}{(N_1 N_2)^3} \left(\langle u_1^\alpha | \partial_{\theta_1} u_2^\alpha \rangle + \langle u_1^\beta | \partial_{\theta_1} u_2^\beta \rangle \right). \quad (27)
\end{aligned}$$

By symmetry, $\text{Tr}(\rho F_U^{\phi_1\phi_2} F_U^{\theta_1\theta_2} - \rho F_U^{\phi_1\theta_1} F_U^{\phi_2\theta_2} + \rho F_U^{\phi_1\theta_2} F_U^{\phi_2\theta_1}) = 3\text{Tr}(\rho F_U^{\phi_1\phi_2} F_U^{\theta_1\theta_2})$, we finally obtain $C_{U_2} = 3$ when $R/\gamma > 1$ and $C_{U_2} = 0$ when $R/\gamma < 1$. Furthermore, the NT (non-topological) second Uhlmann-Chern number $C_{U_2}^{nt}$ is given by

$$C_{U_2}^{nt} = 24R^6 \tanh^5 \frac{E}{T} \int \frac{\sin^6 \theta_1}{(N_1 N_2)^3} \langle u_1^\alpha | \partial_{\theta_1} u_2^\alpha \rangle d\theta_1. \quad (28)$$

In Fig. 7, the NT thermal Uhlmann-Chern number $C_{U_2}^{nt}$ is plotted with respect to the parameter hypersphere radius R and the temperature T , both scaled by γ . The result shows that $C_{U_2}^{nt}$ decreases gradually with increasing thermal noise, but abruptly drops to zero when the radius R is reduced to the regime $R/\gamma < 1$, where the parameter hypersphere no longer encloses the EHS.

V. EXPERIMENTAL FEASIBILITY

Characterizing the mixed-state topology requires three steps. First, the eigenenergies and eigenstates of the NH systems can be extracted using the method from our previous 2D/3D implementations [45, 132] or the protocols

proposed for higher dimensions [48, 49]. Second, at a specific (unknown) temperature, the system is evolved to the thermal equilibrium, and the thermal state is reconstructed via quantum state tomography. The Boltzmann weights are then derived from the tomographic data combined with the extracted eigenenergies and eigenstates. Third, all the thermal topological invariants are computed from the the obtained quantities.

VI. CONCLUSION

We have investigated the mixed-state topology in 2D, 3D and 4D NH systems, associated with the ER, ES and EHS, respectively, which are characterized by the thermal Uhlmann-Chern number, the thermal DD invariant and the second thermal Uhlmann-Chern number. Our results reveal distinctive mixed-state topology absent in pure-state cases, thereby significantly extending the scope of NH topology.

This work was supported by the National Natural Science Foundation of China (Grant Nos. 12475015, 12474356, 12274080, 1187510).

-
- [1] M. Z. Hasan and C. L. Kane, *Rev. Mod. Phys.* **82**, 3045 (2010).
 - [2] X.-L. Qi and S.-C. Zhang, *Rev. Mod. Phys.* **83**, 1057 (2011).
 - [3] S.-Q. Shen, *Topological Insulators: Dirac Equation in Condensed Matters*, Springer Series in Solid-State Sciences, Vol. 174 (Springer Berlin Heidelberg, Berlin, Heidelberg, 2012).
 - [4] B. A. Bernevig, *Topological Insulators and Topological Superconductors* (Princeton University Press, Princeton, 2013).
 - [5] F. D. M. Haldane, *Phys. Rev. Lett.* **61**, 2015 (1988).
 - [6] C. L. Kane and E. J. Mele, *Phys. Rev. Lett.* **95**, 146802 (2005).
 - [7] B. A. Bernevig, T. L. Hughes, and S.-C. Zhang, *Science* **314**, 1757 (2006).
 - [8] M. König, S. Wiedmann, C. Brüne, A. Roth, H. Buhmann, L. W. Molenkamp, X.-L. Qi, and S.-C. Zhang, *Science* **318**, 766 (2007).
 - [9] L. Fu, C. L. Kane, and E. J. Mele, *Phys. Rev. Lett.* **98**, 106803 (2007).
 - [10] L. Fu and C. L. Kane, *Phys. Rev. B* **76**, 045302 (2007).
 - [11] D. Hsieh, D. Qian, L. Wray, Y. Xia, Y. S. Hor, R. J. Cava, and M. Z. Hasan, *Nature* **452**, 970 (2008).
 - [12] C.-K. Chiu, J. C. Y. Teo, A. P. Schnyder, and S. Ryu, *Rev. Mod. Phys.* **88**, 035005 (2016).
 - [13] M. V. Berry, *Proc. R. Soc. A* **392**, 45 (1984).
 - [14] G. Jotzu, M. Messer, R. Desbuquois, M. Lebrat, T. Uehlinger, D. Greif, and T. Esslinger, *Nature* **515**, 237 (2014).
 - [15] P. Roushan, C. Neill, Y. Chen, M. Kolodrubetz, C. Quintana, N. Leung, M. Fang, R. Barends, B. Campbell, Z. Chen, B. Chiaro, A. Dunsworth, E. Jeffrey, J. Kelly, A. Megrant, J. Mutus, P. J. J. O'Malley, D. Sank, A. Vainsencher, J. Wenner, T. White, A. Polkovnikov, A. N. Cleland, and J. M. Martinis, *Nature* **515**, 241 (2014).
 - [16] M. W. Ray, E. Ruokokoski, S. Kandel, M. Möttönen, and D. S. Hall, *Nature* **505**, 657 (2014).
 - [17] P. A. M. Dirac, *Proc. R. Soc. Lond. Ser. A* **133**, 60 (1931).
 - [18] T. Sawada, *Phys. Lett. B* **52**, 67 (1974).
 - [19] R. W. Jackiw, *Int. J. Mod. Phys. A* **19**, 137 (2004).
 - [20] M. D. Schroer, M. H. Kolodrubetz, W. F. Kindel, M. Sandberg, J. Gao, M. R. Vissers, D. P. Pappas, A. Polkovnikov, and K. W. Lehnert, *Phys. Rev. Lett.* **113**, 050402 (2014).
 - [21] X. Tan, D.-W. Zhang, W. Zheng, X. Yang, S. Song, Z. Han, Y. Dong, Z. Wang, D. Lan, H. Yan, S.-L. Zhu, and Y. Yu, *Phys. Rev. Lett.* **126**, 017702 (2021).
 - [22] A. R. Kolovsky, *Phys. Rev. A* **98**, 013603 (2018).
 - [23] M. Nakagawa and N. Kawakami, *Phys. Rev. A* **89**, 013627 (2014).
 - [24] X. S. Wang, A. Brataas, and R. E. Troncoso, *Phys. Rev. Lett.* **125**, 217202 (2020).
 - [25] E. Saei Ghareh Naz, I. C. Fulga, L. Ma, O. G. Schmidt, and J. van den Brink, *Phys. Rev. A* **98**, 033830 (2018).
 - [26] J. Guglielmon, S. Huang, K. P. Chen, and M. C. Rechtsman, *Phys. Rev. A* **97**, 031801 (2018).
 - [27] C. Liu, W. Gao, B. Yang, and S. Zhang, *Phys. Rev. Lett.* **119**, 183901 (2017).
 - [28] C. Dembowski, H.-D. Gräf, H. L. Harney, A. Heine, W. D. Heiss, H. Rehfeld, and A. Richter, *Phys. Rev. Lett.* **86**, 787 (2001).
 - [29] Y. Choi, S. Kang, S. Lim, W. Kim, J.-R. Kim, J.-H. Lee, and K. An, *Phys. Rev. Lett.* **104**, 153601 (2010).

- [30] T. Gao, E. Estrecho, K. Y. Bliokh, T. C. H. Liew, M. D. Fraser, S. Brodbeck, M. Kamp, C. Schneider, S. Höfling, Y. Yamamoto, F. Nori, Y. S. Kivshar, A. G. Truscott, R. G. Dall, and E. A. Ostrovskaya, *Nature* **526**, 554 (2015).
- [31] D. Zhang, X.-Q. Luo, Y.-P. Wang, T.-F. Li, and J. Q. You, *Nat. Commun.* **8**, 1368 (2017).
- [32] C. M. Bender and S. Boettcher, *Phys. Rev. Lett.* **80**, 5243 (1998).
- [33] C. M. Bender, D. C. Brody, and H. F. Jones, *Phys. Rev. Lett.* **89**, 270401 (2002).
- [34] S. K. Özdemir, S. Rotter, F. Nori, and L. Yang, *Nat. Mater.* **18**, 783 (2019).
- [35] A. Guo, G. J. Salamo, D. Duchesne, R. Morandotti, M. Volatier-Ravat, V. Aimez, G. A. Siviloglou, and D. N. Christodoulides, *Phys. Rev. Lett.* **103**, 093902 (2009).
- [36] L. Feng, Z. J. Wong, R.-M. Ma, Y. Wang, and X. Zhang, *Science* **346**, 972 (2014).
- [37] H. Hodaei, M.-A. Miri, M. Heinrich, D. N. Christodoulides, and M. Khajavikhan, *Science* **346**, 975 (2014).
- [38] W. Gou, T. Chen, D. Xie, T. Xiao, T.-S. Deng, B. Gadway, W. Yi, and B. Yan, *Phys. Rev. Lett.* **124**, 070402 (2020).
- [39] W. Liu, Y. Wu, C.-K. Duan, X. Rong, and J. Du, *Phys. Rev. Lett.* **126**, 170506 (2021).
- [40] Z. Ren, D. Liu, E. Zhao, C. He, K. K. Pak, J. Li, and G.-B. Jo, *Nat. Phys.* **18**, 385 (2022).
- [41] X.-L. Zhang, S. Wang, B. Hou, and C. T. Chan, *Phys. Rev. X* **8**, 021066 (2018).
- [42] J. Doppler, A. A. Mailybaev, J. Böhm, U. Kuhl, A. Girschik, F. Libisch, T. J. Milburn, P. Rabl, N. Moiseyev, and S. Rotter, *Nature* **537**, 76 (2016).
- [43] H. Xu, D. Mason, L. Jiang, and J. G. E. Harris, *Nature* **537**, 80 (2016).
- [44] J. W. Yoon, Y. Choi, C. Hahn, G. Kim, S. H. Song, K.-Y. Yang, J. Y. Lee, Y. Kim, C. S. Lee, J. K. Shin, H.-S. Lee, and P. Berini, *Nature* **562**, 86 (2018).
- [45] P.-R. Han, F. Wu, X.-J. Huang, H.-Z. Wu, C.-L. Zou, W. Yi, M. Zhang, H. Li, K. Xu, D. Zheng, H. Fan, J. Wen, Z.-B. Yang, and S.-B. Zheng, *Phys. Rev. Lett.* **131**, 260201 (2023).
- [46] W. Chen, S. Kaya Özdemir, G. Zhao, J. Wiersig, and L. Yang, *Nature* **548**, 192 (2017).
- [47] H. Hodaei, A. U. Hassan, S. Wittek, H. Garcia-Gracia, R. El-Ganainy, D. N. Christodoulides, and M. Khajavikhan, *Nature* **548**, 187 (2017).
- [48] S.-B. Yang, P.-R. Han, W. Ning, F. Wu, Z.-B. Yang, and S.-B. Zheng, *Sci. China Phys. Mech* **69**, 230313 (2026).
- [49] S.-B. Yang, P.-R. Han, W. Ning, F. Wu, Z.-B. Yang, and S.-B. Zheng, “A hypersphere-like non-abelian yang monopole and its topological characterization,” (2025), arXiv:2510.00941 [quant-ph].
- [50] E. J. Bergholtz, J. C. Budich, and F. K. Kunst, *Rev. Mod. Phys.* **93**, 015005 (2021).
- [51] K. Ding, C. Fang, and G. Ma, *Nat. Rev. Phys.* **4**, 745 (2022).
- [52] M.-A. Miri and A. Alù, *Science* **363**, eaar7709 (2019).
- [53] Y. Xu, S.-T. Wang, and L.-M. Duan, *Phys. Rev. Lett.* **118**, 045701 (2017).
- [54] T. Yoshida, R. Peters, N. Kawakami, and Y. Hatsugai, *Phys. Rev. B* **99**, 121101 (2019).
- [55] T. Liu, J. J. He, Z. Yang, and F. Nori, *Phys. Rev. Lett.* **127**, 196801 (2021).
- [56] S. A. A. Ghorashi, T. Li, and M. Sato, *Phys. Rev. B* **104**, L161117 (2021).
- [57] R. L. Mc Guinness and P. R. Eastham, *Phys. Rev. Res.* **2**, 043268 (2020).
- [58] T. Matsushita, Y. Nagai, and S. Fujimoto, *Phys. Rev. B* **100**, 245205 (2019).
- [59] J.-j. Liu, Z.-w. Li, Z.-G. Chen, W. Tang, A. Chen, B. Liang, G. Ma, and J.-C. Cheng, *Phys. Rev. Lett.* **129**, 084301 (2022).
- [60] B. Zhen, C. W. Hsu, Y. Igarashi, L. Lu, I. Kaminer, A. Pick, S.-L. Chua, J. D. Joannopoulos, and M. Soljačić, *Nature* **525**, 354 (2015).
- [61] A. Cerjan, S. Huang, M. Wang, K. P. Chen, Y. Chong, and M. C. Rechtsman, *Nat. Photonics* **13**, 623 (2019).
- [62] W. Tang, K. Ding, and G. Ma, *Nat. Commun.* **14**, 6660 (2023).
- [63] H. Zhou, J. Y. Lee, S. Liu, and B. Zhen, *Optica* **6**, 190 (2019).
- [64] X. Zhang, K. Ding, X. Zhou, J. Xu, and D. Jin, *Phys. Rev. Lett.* **123**, 237202 (2019).
- [65] J. J. Sakurai and J. Napolitano, *Modern quantum mechanics*, 2nd ed. (Addison-Wesley, Pearson, Boston, Mass., 2011).
- [66] A. Coser and D. Pérez-García, *Quantum* **3**, 174 (2019).
- [67] L. A. Lessa, M. Cheng, and C. Wang, *Phys. Rev. X* **15**, 011069 (2025).
- [68] H. Xue, J. Y. Lee, and Y. Bao, “Tensor network formulation of symmetry protected topological phases in mixed states,” (2024), arXiv:2403.17069 [cond-mat.str-el].
- [69] R. Ma and A. Turzillo, *PRX Quantum* **6**, 010348 (2025).
- [70] Z. Zhang, U. Agrawal, and S. Vijay, *Phys. Rev. B* **111**, 115141 (2025).
- [71] J. Shah, C. Fechisin, Y.-X. Wang, J. T. Iosue, J. D. Watson, Y.-Q. Wang, B. Ware, A. V. Gorshkov, and C.-J. Lin, “Instability of steady-state mixed-state symmetry-protected topological order to strong-to-weak spontaneous symmetry breaking,” (2024), arXiv:2410.12900 [quant-ph].
- [72] S. Sun, J.-H. Zhang, Z. Bi, and Y. You, *PRX Quantum* **6**, 020333 (2025).
- [73] Y. You and M. Oshikawa, *Phys. Rev. B* **110**, 165160 (2024).
- [74] Y. Guo, J.-H. Zhang, H.-R. Zhang, S. Yang, and Z. Bi, *Phys. Rev. X* **15**, 021060 (2025).
- [75] S. Sang, Y. Zou, and T. H. Hsieh, *Phys. Rev. X* **14**, 031044 (2024).
- [76] K. Su, Z. Yang, and C.-M. Jian, *Phys. Rev. B* **110**, 085158 (2024).
- [77] Z. Li and R. S. K. Mong, *Phys. Rev. B* **111**, 125106 (2025).
- [78] S. Sang and T. H. Hsieh, *Phys. Rev. Lett.* **134**, 070403 (2025).
- [79] J. Hauser, Y. Bao, S. Sang, A. Lavasani, U. Agrawal, and M. P. A. Fisher, “Information dynamics in decohered quantum memory with repeated syndrome measurements: a dual approach,” (2024), arXiv:2407.07882 [quant-ph].
- [80] A.-R. Negari, T. D. Ellison, and T. H. Hsieh, “Space-time markov length: a diagnostic for fault tolerance via mixed-state phases,” (2025), arXiv:2412.00193 [quant-

- ph].
- [81] S. Lee and E.-G. Moon, *PRX Quantum* **6**, 030355 (2025).
- [82] Y. Bao, R. Fan, A. Vishwanath, and E. Altman, “Mixed-state topological order and the errorfield double formulation of decoherence-induced transitions,” (2023), [arXiv:2301.05687](https://arxiv.org/abs/2301.05687) [quant-ph].
- [83] R. Fan, Y. Bao, E. Altman, and A. Vishwanath, *PRX Quantum* **5**, 020343 (2024).
- [84] R. Ma, J.-H. Zhang, Z. Bi, M. Cheng, and C. Wang, *Phys. Rev. X* **15**, 021062 (2025).
- [85] T.-C. Lu, Z. Zhang, S. Vijay, and T. H. Hsieh, *PRX Quantum* **4**, 030318 (2023).
- [86] Y.-H. Chen and T. Grover, *Phys. Rev. Lett.* **132**, 170602 (2024).
- [87] Y.-H. Chen and T. Grover, *Phys. Rev. B* **110**, 125152 (2024).
- [88] Z. Wang, Z. Wu, and Z. Wang, *PRX Quantum* **6**, 010314 (2025).
- [89] K. Su, N. Myerson-Jain, and C. Xu, *Phys. Rev. B* **109**, 035146 (2024).
- [90] T.-C. Lu, *Phys. Rev. B* **110**, 125145 (2024).
- [91] R. Sohal and A. Prem, *PRX Quantum* **6**, 010313 (2025).
- [92] T. D. Ellison and M. Cheng, *PRX Quantum* **6**, 010315 (2025).
- [93] P. Sala and R. Verresen, *Phys. Rev. Lett.* **134**, 250403 (2025).
- [94] Y. Kim, A. Lavasani, and S. Vijay, “Persistent topological negativity in a high-temperature mixed-state,” (2025), [arXiv:2408.00066](https://arxiv.org/abs/2408.00066) [quant-ph].
- [95] Q. Wang, B. Wang, J. Wang, and L. Zhang, *Chin. Phys. Lett.* **42**, 070603 (2025).
- [96] Y.-H. Chen and T. Grover, *PRX Quantum* **5**, 030310 (2024).
- [97] L. A. Lessa, R. Ma, J.-H. Zhang, Z. Bi, M. Cheng, and C. Wang, *PRX Quantum* **6**, 010344 (2025).
- [98] P. Sala, S. Gopalakrishnan, M. Oshikawa, and Y. You, *Phys. Rev. B* **110**, 155150 (2024).
- [99] D. Gu, Z. Wang, and Z. Wang, “Spontaneous symmetry breaking in open quantum systems: strong, weak, and strong-to-weak,” (2024), [arXiv:2406.19381](https://arxiv.org/abs/2406.19381) [quant-ph].
- [100] C. Zhang, Y. Xu, J.-H. Zhang, C. Xu, Z. Bi, and Z.-X. Luo, *Phys. Rev. B* **111**, 115137 (2025).
- [101] J. Kim, E. Altman, and J. Y. Lee, “Error threshold of syk codes from strong-to-weak parity symmetry breaking,” (2024), [arXiv:2410.24225](https://arxiv.org/abs/2410.24225) [quant-ph].
- [102] X. Huang, M. Qi, J.-H. Zhang, and A. Lucas, *Phys. Rev. B* **111**, 125147 (2025).
- [103] R. Luo, Y.-N. Wang, and Z. Bi, *PRX Quantum* **6**, 040358 (2025).
- [104] A. Uhlmann, *Rep. Math. Phys.* **24**, 229 (1986).
- [105] A. Uhlmann, *Lett. Math. Phys.* **21**, 229 (1991).
- [106] A. Uhlmann, *Rep. Math. Phys.* **33**, 253 (1993).
- [107] E. Sjöqvist, A. K. Pati, A. Ekert, J. S. Anandan, M. Ericsson, D. K. L. Oi, and V. Vedral, *Phys. Rev. Lett.* **85**, 2845 (2000).
- [108] M. Ericsson, A. K. Pati, E. Sjöqvist, J. Brännlund, and D. K. L. Oi, *Phys. Rev. Lett.* **91**, 090405 (2003).
- [109] J. Åberg, D. Kult, E. Sjöqvist, and D. K. L. Oi, *Phys. Rev. A* **75**, 032106 (2007).
- [110] J. Zhu, M. Shi, V. Vedral, X. Peng, D. Suter, and J. Du, *Europhys. Lett.* **94**, 20007 (2011).
- [111] J. C. Budich and S. Diehl, *Phys. Rev. B* **91**, 165140 (2015).
- [112] O. Andersson, I. Bengtsson, M. Ericsson, and E. Sjöqvist, *Philos. Trans. R. Soc. A* **374**, 20150231 (2016).
- [113] B. Mera, C. Vlachou, N. Paunković, and V. R. Vieira, *J. Phys. A: Math. Theor.* **50**, 365302 (2017).
- [114] B. Mera, C. Vlachou, N. Paunković, and V. R. Vieira, *Phys. Rev. Lett.* **119**, 015702 (2017).
- [115] O. Viyuela, A. Rivas, and M. A. Martin-Delgado, *Phys. Rev. Lett.* **112**, 130401 (2014).
- [116] Y. He and C.-C. Chien, *Phys. Rev. B* **106**, 024310 (2022).
- [117] Y. He, H. Guo, and C.-C. Chien, *Phys. Rev. B* **97**, 235141 (2018).
- [118] X. Wang, X.-Y. Hou, Y. He, and H. Guo, *Phys. Rev. B* **112**, 214112 (2025).
- [119] Y. R. Kartik and S. Sarkar, *Sci. Rep.* **13**, 6431 (2023).
- [120] A. Pi, Y. Zhang, Y. He, and C.-C. Chien, *Phys. Rev. B* **105**, 085418 (2022).
- [121] P. Molignini and N. R. Cooper, *Phys. Rev. Res.* **5**, 023004 (2023).
- [122] C.-E. Bardyn, L. Wawer, A. Altland, M. Fleischhauer, and S. Diehl, *Phys. Rev. X* **8**, 011035 (2018).
- [123] X.-Y. Hou, X. Wang, Z. Zhou, H. Guo, and C.-C. Chien, *Phys. Rev. B* **107**, 165415 (2023).
- [124] S. Liu, *Quantum Inf. Process.* **21**, 383 (2022).
- [125] A. Carollo, B. Spagnolo, and D. Valenti, *Sci. Rep.* **8**, 9852 (2018).
- [126] O. Viyuela, A. Rivas, S. Gasparinetti, A. Wallraff, S. Filipp, and M. A. Martin-Delgado, *npj Quantum Inf.* **4**, 10 (2018).
- [127] M. Gell-Mann, *Phys. Rev.* **125**, 1067 (1962).
- [128] R. I. Nepomechie, *Phys. Rev. D* **31**, 1921 (1985).
- [129] M. Chen, C. Li, G. Palumbo, Y.-Q. Zhu, N. Goldman, and P. Cappellaro, *Science* **375**, 1017 (2022).
- [130] M. Hübner, *Phys. Lett. A* **179**, 226 (1993).
- [131] S. Sugawa, F. Salces-Carcoba, A. R. Perry, Y. Yue, and I. B. Spielman, *Science* **360**, 1429 (2018).
- [132] P.-R. Han, W. Ning, X.-J. Huang, R.-H. Zheng, S.-B. Yang, F. Wu, Z.-B. Yang, Q.-P. Su, C.-P. Yang, and S.-B. Zheng, *Nat. Commun.* **15**, 10293 (2024).